Simulation of Quantum Interference and Non-Markovian Emission Dynamics Induced by Localized Exciton-Polaritons

IOANNIS THANOPULOS, VASILIOS KARANIKOLAS, EMMANUEL PASPALAKIS
University of Patras
Materials Science Department
Patras 265 04
Greece
ithano@upatras.gr, karanikv@tcd.ie, paspalak@upatras.gr

Abstract: We analyze the spontaneous emission dynamics of a V-type quantum emitter close to a molybdenum disulfide (MoS_2) nanodisk. We show that a MoS_2 nanodisk leads to both high-degree quantum interference and non-Markovian dynamics in the spontaneous emission of the nearby quantum emitter. We analyze the spontaneous emission dynamics by combining quantum dynamics calculations with electromagnetic calculations. A rich population dynamics ranging from decaying Rabi oscillations to complex decaying oscillations and strong population exchange between the upper states of the quantum emitter is obtained depending on the parameters of the system. Our results have potential applications in quantum technologies.

Key–Words: Quantum emitter, MoS_2 nanodisk, Exciton-polaritons, Spontaneous emission, Quantum interference, Non-Markovian dynamics

1 Introduction

Three-level quantum emitters (QEs) give important quantum coherence and interference effects [1] and may be particularly important in quantum technologies. A basic three-level emitter is the V-type QE (see Fig. 1) where one may simulate quantum interference effects in spontaneous emission (SE) [1, 2] by placing the QE in a photonic environment with anisotropic Purcell effect [3]. The quantum interference in SE allows for coupling between the two upper states of the V-type emitter in the anisotropic vacuum, while in the ordinary vacuum no coupling occurs. This phenomenon has been explored, mainly under Markovian spontaneous decay dynamics, next to several photonic structures, including negative-index metamaterials [4, 5] and metasurfaces [6], plasmonic nanostructures [7, 8, 9], and semiconductor microcavities [10].

Non-Markovian effects in quantum interference in the SE dynamics of a QE have been recently studied in a V-type QE next to a 5 nm radius silver spherical nanoparticle [11] and next to a 30 nm radius MoS_2 nanodisk (ND) [12]. There, strong non-Markovian response was shown for the QE close to the nanostructures. MoS_2 is an atomically thin, direct band gap semiconducting two-dimensional material [13, 14] featuring bandgap in the visible, with strong excitonic resonances and high oscillator strengths that can support exciton-polaritons [15, 16, 17]. MoS_2 has lower material losses than noble metals and when the transverse magnetic surface exciton-polariton modes are excited the total normalized SE rate of a nearby QE is enhanced by several orders of magnitude compared with its free-space value [16]. The confinement of the transverse magnetic exciton-polariton mode from an infinite MoS_2 layer to a MoS_2 ND, leads to a redistribution of the available hybrid EM modes leading to localized exciton-polariton modes and then sharp peaks of the Purcell enhancement factor emerge [17]. In this study, we combine quantum dynamics calculations with electromagnetic (EM) calculations and explore further the decay dynamics of a V-type QE located near a MoS_2 ND for different parameters of the system than those used in our previous study [12].

2 Theory

We consider a V-type QE with two degenerate excited states located at $\vec{r} = (0, 0, z)$ of a coordinate system with origin at the center of the ND, as shown in Fig. 1. The transition electric dipole moments of the QE are $\vec{\mu}_{10} = \mu\hat{\varepsilon}_-$ and $\vec{\mu}_{20} = \mu\hat{\varepsilon}_+$, where $\hat{\varepsilon}_\pm \equiv (\hat{\varepsilon}_z \pm i\hat{\varepsilon}_{x(y)})/\sqrt{2}$ describe the right-rotating ($\hat{\varepsilon}_+$) and left-rotating ($\hat{\varepsilon}_-$) unit vectors (μ is taken to be real). Also, ω_0 stands for the resonance frequency between the two degenerate excited states and the lower state in the V-type QE, where the energy of the lower state is taken as zero.

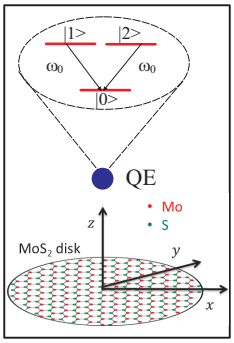

Figure 1: A V-type QE with resonance frequency ω_0 placed at a distance $z = D$ perpendicular from the center of a nanodisk of radius R.

The state of the system is given by

$$|\Psi(t)\rangle = c_1(t)e^{-i\omega_0 t}|1;0_\omega\rangle + c_2(t)e^{-i\omega_0 t}|2;0_\omega\rangle + \int d\vec{r}\int d\omega\, C(\vec{r},\omega,t)e^{-i\omega t}|0;1_{\vec{r},\omega}\rangle \quad (1)$$

Here, $|n;a\rangle = |n\rangle \otimes |a\rangle$, where $|n\rangle$ $(n = 0, 1, 2)$ denotes the quantum states of the V-type QE, see Fig. 1, and $|a\rangle$ denotes the photonic states of the modified EM modes due to the presence of the ND, with $|0_\omega\rangle$ standing for the vacuum and $|1_{\vec{r},\omega}\rangle$ for one photon states. The equation for $c_1(t)$ and $c_2(t)$ are given by (we use $\hbar = 1$ in this paper) [11]

$$\dot{c}_1(t) = i\int_0^t dt'\Big(K^+(t-t')c_1(t') + K^-(t-t')c_2(t')\Big), \quad (2)$$

$$\dot{c}_2(t) = i\int_0^t dt'\Big(K^-(t-t')c_1(t') + K^+(t-t')c_2(t')\Big), \quad (3)$$

where

$$K^\pm(t-t') = i\int_0^\infty \tilde{J}^\pm(\omega)e^{-i(\omega-\omega_0)(t-t')}d\omega\,, \quad (4)$$

with

$$\tilde{J}^\pm(\omega) = \frac{\Gamma_0(\omega_0)}{4\pi}\left[\lambda^\perp(\omega,D) \pm \lambda^\parallel(\omega,D)\right](\frac{\omega}{\omega_0})^3\,, \quad (5)$$

with $\Gamma_0(\omega_0)$ standing for the free-space decay width of the QE, and $\lambda^k(\omega,D) \equiv \Gamma^k(\omega)/\Gamma_0(\omega)$ is the directional ($k = \perp, \parallel$) Purcell enhancement factor of the free-space decay rate due to the presence of the ND at $z = D$ from the QE. We compute the upper level population dynamics of the QE $|c_1(t)|^2$ and $|c_2(t)|^2$ by using the effective mode differential equation (EMDE) methodology [11].

We calculate the Purcell factor of the QE due to the presence of the ND, where the calculation of the EM Green's tensor is the most crucial quantity needed. The relation between the transition dipole moments and the free-space decay width is given by $\Gamma_0(\omega) = \frac{\omega_0^3\mu^2}{3\pi\epsilon_0 c^3}(\frac{\omega}{\omega_0})^3 = \Gamma_0(\omega_0)(\frac{\omega}{\omega_0})^3$ [11]. In the presented calculations, the QE is always located on the axis of rotational symmetry of the ND, implying $\vec{r}_{QE} = (0,0,z)$. We calculate the directional Purcell factors given by

$$\lambda^k(\omega,\vec{r}) = \sqrt{\varepsilon} + \frac{6\pi c}{\omega}\mathrm{Im}\,\hat{\mathbf{G}}_k(\vec{r},\vec{r},\omega),\ k = \perp, \parallel \quad (6)$$

where ε is the permittivity of the host medium, $\hat{\mathbf{G}}_\parallel \equiv \hat{\mathbf{G}}_{xx(yy)}$ and $\hat{\mathbf{G}}_\perp \equiv \hat{\mathbf{G}}_{zz}$ are the induced parts of the EM Green's tensor, due to the ND, calculated at the QE position [18]. We deal with the near field regime of the QE, for which the QE separation from the MoS_2 ND is much smaller than the SE wavelength of the QE, $|\vec{r}| \ll \lambda$. Thus, we can use the electrostatic approximation.

For the QE in an isotropic vacuum $\lambda^\perp(\omega,\vec{r}) = \lambda^\parallel(\omega,\vec{r})$, so $\tilde{J}^- = 0$ leading to $K^-(t-t') = 0$, and there is no coupling between states $|1\rangle$ and $|2\rangle$. In this case each state is coupled independently to the EM continuum. However, under anisotropic Purcell enhancement factors with $\lambda^\perp(\omega,\vec{r}) \neq \lambda^\parallel(\omega,\vec{r})$ coupling between the two upper states is created leading to population transfer between the two upper states, a phenomenon that changes significantly the QE population dynamics. This can happen when placing the QE near a MoS_2 ND.

We consider a free-standing MoS_2 disk, with host medium dielectric permittivity $\varepsilon = 1$. The induced parts of the EM Green's tensor are given by [17]:

$$\hat{\mathbf{G}}_{xx(yy)}(z,\omega) = \mathcal{F}\sum_{n=0}^{\infty} c_n^1(z,\omega)\frac{\left[\tilde{\mathcal{R}} - z/R\right]^{2n+2}}{\tilde{\mathcal{R}}}, \quad (7)$$

$$\hat{\mathbf{G}}_{zz}(z,\omega) = \pm\mathcal{F}\sum_{n=0}^{\infty} c_n^0(z,\omega)\frac{\left[\tilde{\mathcal{R}} - z/R\right]^{2n+1}}{\tilde{\mathcal{R}}}, \quad (8)$$

with $\tilde{\mathcal{R}} = \sqrt{(z/R)^2+1}$ and $\mathcal{F} = -c^2/2\omega^2$. The expansion coefficients $c_n^0(z,\omega)$ and $c_n^1(z,\omega)$ are obtained as solutions of a matrix equation, where their values depend on the position of the QE, the angular eigenmodes $l = 0, 1$ and the radial eigenmode n [17]. The surface conductivity of MoS_2, $\sigma_{MoS_2}(\omega)$, which is needed in the calculation of the Green's tensor, is described by the model presented in Refs. [17, 19].

In case that $\tilde{J}^{\pm}(\omega)$ has a Lorentzian form

$$J^{L}(\omega)=\frac{1}{4\pi}\frac{\Gamma_0(\omega_0)\lambda(\omega_0,D)\beta^2}{(\omega_0-\omega-\Delta)^2+\beta^2}, \tag{9}$$

with either $\lambda(\omega_0,D)=\lambda^{\perp}(\omega_0,D)$ or $\lambda(\omega_0,D)=\lambda^{\parallel}(\omega_0,D)$, $\Delta\equiv\omega_0-\omega_c$ being the detuning between the QE frequency ω_0 and a cavity-like central mode frequency ω_c, and β denoting the spectral width of the coupling to the central mode, the upper levels population dynamics of the QE can be now calculated analytically for specific initial states. In particular, for an antisymmetric initial state, $|\psi^A(0)\rangle=\sqrt{0.5}|1;0_\omega\rangle-\sqrt{0.5}|2;0_\omega\rangle$, the upper states population time evolution is given by

$$\begin{aligned}|C_1^A(t)|^2 &= |C_2^A(t)|^2 \\ &= \left|\frac{e^{-0.5\tilde{\beta}t}}{\sqrt{2}}\left[\cosh\left(\frac{q^At}{2}\right)\right.\right. \\ &+ \left.\left.\frac{\tilde{\beta}}{q^A}\sinh\left(\frac{q^At}{2}\right)\right]\right|^2\end{aligned} \tag{10}$$

with $\tilde{\beta}=\beta-i\Delta$, and $q^A=\sqrt{\tilde{\beta}^2-2\Gamma_0(\omega_0)\lambda^{\parallel}(\omega_0,D)\beta}$.

3 Numerical results

In the upper panel of Fig. 2 we depict the Purcell enhancement factors $\lambda^{\perp}(\omega,D)=\Gamma^z(\omega)/\Gamma_0(\omega)$ and $\lambda^{\parallel}(\omega,D)=\Gamma^x(\omega)/\Gamma_0(\omega)$ taking the transition dipole moments along the z and x directions, respectively, where the QE is located at distance $z=5,15$ nm from the center of a MoS_2 ND of radius $R=7.5$ nm. The decay rate is significantly enhanced, for about four orders of magnitude, at specific energies. Also, depending on the distance of the QE from the ND and the direction of the transition dipole moment, different peaks appear in the Purcell enhancement factors. The strong and sharp peaks in the Purcell factors correspond to the localized exciton-polariton resonances supported by the MoS_2 ND. The MoS_2 ND supports localized-exciton modes at the resonance frequencies ω_n^l, which are found by numerically solving the equation $\sigma_{MoS_2}(\omega_n^l)/\omega_n^l=2i\varepsilon_0 R/\zeta_n^l$, where ζ_n^l are the geometric eigenmodes [20]. The different transition dipole moment orientations of the QE excite different set of localized exciton-polariton modes ($l=0$ for the z orientation and $l=1$ for the x orientation) when the QE is placed above (or below) the center of ND. When we increase the distance between the QE and the ND, the strength of the interaction weakens, because the near-field of the QE decouples from the ND.

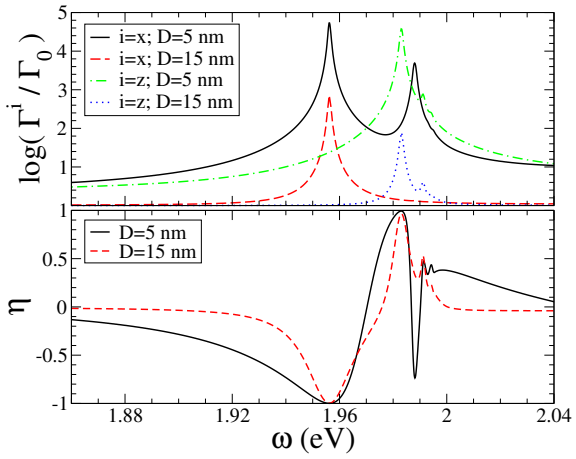

Figure 2: Upper: Purcell factor $\lambda^{\perp}(\omega,D)=\Gamma^z(\omega)/\Gamma_0(\omega)$ and $\lambda^{\parallel}(\omega,D)=\Gamma^x(\omega)/\Gamma_0(\omega)$ of a QE at distances $D=5$ nm and $D=15$ nm from a MoS_2 ND with radius $R=7.5$ nm along the perpendicular (z) and parallel (x) direction to the ND. Lower: The quantum interference factor $\eta(\omega,D)$ of a QE at distances $D=5$ nm and $D=15$ nm from a MoS_2 ND with radius $R=7.5$ nm.

We also present the quantum interference factor

$$\eta(\omega,D)\equiv\frac{\Gamma^z(\omega)-\Gamma^x(\omega)}{\Gamma^z(\omega)+\Gamma^x(\omega)}. \tag{11}$$

in Fig. 2 (lower panel). We note that the quantum interference factor reaches values very close to -1 and 1, which are the values that give maximum quantum interference [1, 2], at different energies and distances from the ND. This is in contrast to the plasmonic nanosphere where the maximum values of the quantum interference factor is about 0.7 [11]. This happens as in the MoS_2 ND the exciton-polariton resonances for transition dipole moments perpendicular or parallel to the MoS_2 ND occur at different resonance frequencies, leading to strongly non-overlapping Purcell enhancement factors along the two different dipole directions. Here, we consider QEs with $\Gamma_0(\omega_0)=0.05$ meV and with ω_0 leading to quantum interference factor $\eta\approx-1$, in order to explore the effects of maximum quantum interference.

We now turn to the spontaneous emission dynamics by solving numerically Eqs. (2) and (3). In Fig. 3, we present the dynamics of a V-type QE with resonance frequency $\omega_0=1.956$ eV located at $D=15$ nm from the ND with $R=7.5$ nm. In the upper panel, the $|c_1(t)|^2$ (black solid curve) and the $|c_2(t)|^2$ (red dashed curve) are shown for a QE with initial

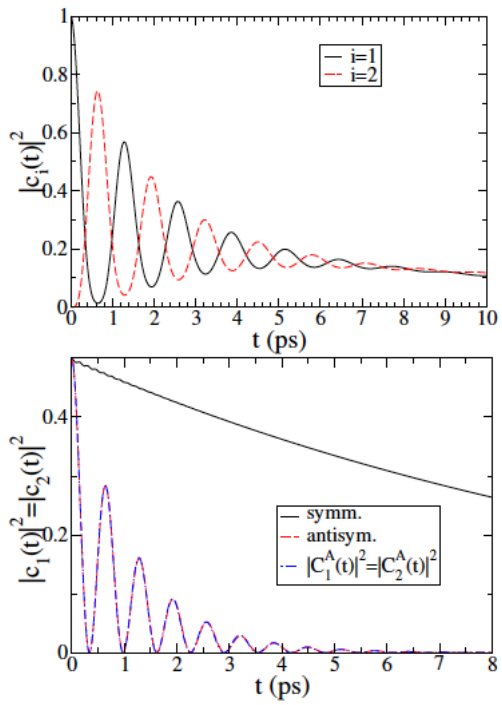

Figure 3: (color online) Dynamics of a V-type QE with free-space decay width $\Gamma_0 = 0.05$ meV and resonance frequency $\omega_0 = 1.956$ eV located at $z = 15$ nm from a MoS_2 disk with radius $R = 7.5$ nm. Upper panel: The $|c_1(t)|^2$ (black solid curve) and $|c_2(t)|^2$ (red dashed curve) for an initial state $|\Psi(0)\rangle = |1;0_\omega\rangle$. Lower panel: The $|c_1(t)|^2 = |c_2(t)|^2$ for a symmetric initial state $|\Psi^S(0)\rangle$ (black solid curve) and an antisymmetric initial state $|\Psi^A(0)\rangle$ (red dashed curve), as well as the $|C_1^A(t)|^2 = |C_2^A(t)|^2$ for an antisymmetric initial state (blue dot-dashed curve) given by Eq. (10).

state $|\Psi(0)\rangle = |1;0_\omega\rangle$. We find significant population transfer between the two upper states at early times accompanied with strong decaying Rabi oscillations where more than 80% of the initial population decays out into the EM continuum of modes within about 10 ps. In the lower panel of Fig. 3 we show the $|c_1(t)|^2 = |c_2(t)|^2$ for a symmetric $|\psi^S(0)\rangle = \sqrt{0.5}|1;0_\omega\rangle + \sqrt{0.5}|2;0_\omega\rangle$ (black solid curve) and an antisymmetric $|\psi^A(0)\rangle = \sqrt{0.5}|1;0_\omega\rangle - \sqrt{0.5}|2;0_\omega\rangle$ (red dashed curve) initial state. We find that the decay for a symmetric initial state takes place on a much longer scale than for an antisymmetric initial state, although the coupling conditions between the QE and the exciton-polariton resonances are identical in both cases. Moreover, for the symmetric initial state the decay exhibits weak non-Markovian features with small oscillations on top of the decay dynamics. In contrast, the decay of an antisymmetric initial state has strong non-Markovian character; the QE population $|c_1(t)|^2 = |c_2(t)|^2$ oscillates completely between the QE and the EM continuum of modes, with decaying Rabi oscillations, and it decays gradually in total into the EM continuum within about 6 ps. In the lower panel of Fig. 3, we also show the QE population time evolution for an antisymmetric initial state computed analytically $|C_1^A(t)|^2 = |C_2^A(t)|^2$ (blue dot-dashed curve) using Eq. (10) after fitting a single peak Lorentzian profile to $J^{\pm}(\omega)$ using $J^L(\omega)$ at the coupling conditions for a QE at $D = 15$ nm distance from the ND of radius $R = 7.5$ nm [21]. The analytically computed population dynamics is in excellent agreement with the corresponding exact dynamics $|c_1(t)|^2 = |c_2(t)|^2$ obtained by the EMDE methodology.

In Fig. 4 we show the dynamics of a V-type QE with free-space decay width $\Gamma_0 = 0.05$ meV and resonance frequency $\omega_0 = 1.956$ eV located at $z = 5$ nm from a MoS_2 disk with radius $R = 7.5$ nm. The upper panel shows the $|c_1(t)|^2$ (black solid curve) and $|c_2(t)|^2$ (red dashed curve) for an initial state $|\Psi(0)\rangle = |1;0_\omega\rangle$. We find that the initial population oscillates rapidly between state $|1\rangle$ and state $|2\rangle$, while overall it decays totally within about 8 ps into the modified by the ND continuum of EM modes. The fact that the population oscillates completely between the two upper states of the QE during the overall decay process is a direct indication that the QE is resonant to an exciton-polaron resonance in the ND. High-frequency oscillations with decaying amplitude on top of the overall decay dynamics are due to the overlapping of the exciton-polariton resonance at $\omega_0 = 1.956$ eV with the next one higher in energy, according to the peaks in the Purcell factors shown in Fig. 2.

4 Conclusions

In conclusion, we have studied the SE dynamics of a V-type QE near a MoS_2 ND. The anisotropic photonic environment created by the localized exciton-polaritons of the ND results to interference effects in SE leading to coupling and population transfer between the two upper states. This is also complimented by non-Markovian SE dynamics. Effects such as decaying Rabi oscillations and complex decaying oscillations may occur. The SE dynamics for given coupling conditions between the QE and the ND, depends crucially on the initial state of the QE. An analytical solution for the population dynamics, which gives good agreement with the simulations in certain cases

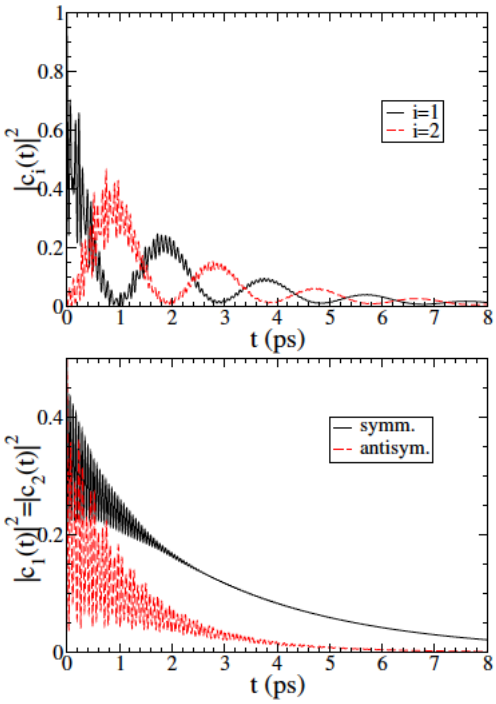

Figure 4: (color online) Dynamics of a V-type QE with free-space decay width $\Gamma_0 = 0.05$ meV and resonance frequency $\omega_0 = 1.956$ eV located at $z = 5$ nm from a MoS_2 disk with radius $R = 7.5$ nm. Upper panel: The $|c_1(t)|^2$ (black solid curve) and $|c_2(t)|^2$ (red dashed curve) for an initial state $|\Psi(0)\rangle = |1; 0_\omega\rangle$. Lower panel: The $|c_1(t)|^2 = |c_2(t)|^2$ for a symmetric initial state $|\Psi^S(0)\rangle$ (black solid curve) and an antisymmetric initial state $|\Psi^A(0)\rangle$ (red dashed curve) are shown.

is also presented. Moreover, results for different ND radii, different QE free-space decay widths, and different, off-axis, positioning of the QE have been obtained (not shown in the paper, but will be shown during the presentation), which show similar qualitative behavior as the one presented here. Our results could be useful in the development of novel nanophotonic devices, as well as, future quantum technologies.

Acknowledgements: Co-financed by Greece and the European Union—European Regional Development Fund via the General Secretariat for Research and Technology bilateral Greek-Russian Science and Technology collaboration project on Quantum Technologies (project code name POLISIMULATOR).

References:

[1] Z. Ficek and S. Swain, *Quantum Interference and Coherence: Theory and Experiments*, Springer–Verlag, New York, 2005.

[2] M. Kiffner, M. Macovei, J. Evers, and C. H. Keitel, Vacuum-induced processes in multi-level atoms, *Prog. Opt.* 55, 2010, pp. 85–197.

[3] G. S. Agarwal, Anisotropic vacuum-induced interference in decay channels, *Phys. Rev. Lett.* 84, 2000, pp. 5500–5503.

[4] Y.-P. Yang, J.-P. Xu, H. Chen, and S.-Y. Zhu, Quantum interference enhancement with left-handed materials, *Phys. Rev. Lett.* 100, 2008, art. no. 043601.

[5] G.-X. Li, J. Evers, and C. H. Keitel, Spontaneous emission interference in negative-refractive-index waveguides, *Phys. Rev. B* 80, 2009, art. no. 045102.

[6] P. K. Jha, X. Ni, C. Wu, Y. Wang, and X. Zhang, Metasurface-enabled remote quantum interference, *Phys. Rev. Lett.* 115, 2015, art. no. 025501.

[7] V. Yannopapas, E. Paspalakis, and N. V. Vitanov, Plasmon-induced enhancement of quantum interference near metallic nanostructures, *Phys. Rev. Lett.* 103, 2009, art. no. 063602.

[8] S. Evangelou, V. Yannopapas, and E. Paspalakis, Simulating quantum interference in spontaneous decay near plasmonic nanostructures: population dynamics. *Phys. Rev. A* 83, 2011, art. no. 055805.

[9] V. Karanikolas and E. Paspalakis, Plasmon–induced quantum interference near carbon nanostructures, *J. Phys. Chem. C* 122, 2018, 14788.

[10] S. Hughes and G. S. Agarwal, Anisotropy-induced quantum interference and population trapping between orthogonal quantum dot exciton states in semiconductor cavity systems, *Phys. Rev. Lett.* 118, 2017, art. no. 063601.

[11] I. Thanopulos, V. Yannopapas, and E. Paspalakis, Non-Markovian dynamics in plasmon-induced spontaneous emission interference, *Phys. Rev. B* 95, 2017, art. no. 075412.

[12] I. Thanopulos, V. Karanikolas, and E. Paspalakis, Non-Markovian spontaneous emission interference near a MoS_2 nanodisk, *Opt. Lett.* 99, 2019, pp. 3510–3513.

[13] K. F. Mak, C. Lee, J. Hone, J. Shan, and T. F. Heinz, Atomically thin MoS_2: a new direct-gap semiconductor, *Phys. Rev. Lett.* 105, 2010, art. no. 136805.

[14] K. F. Mak and J. Shan, Photonics and optoelectronics of 2D semiconductor transition metal dichalcogenides, *Nature Photonics* 10, 2016, pp. 216–226 .

[15] D. N. Basov, M M. Fogler, and F. J. G. de Abajo, Polaritons in van der Waals materials, *Science* 354, 2016, art. no. aag1992.

[16] V. D. Karanikolas, C. A. Marocico, P. R. Eastham, and A. L. Bradley, Near–field relaxation of a quantum emitter to two-dimensional semiconductors: Surface dissipation and exciton polaritons, *Phys. Rev. B* 94, 2016, art. no. 195418.

[17] V. D. Karanikolas and E. Paspalakis, Localized exciton modes and high quantum efficiency of a quantum emitter close to a MoS_2 nanodisk, *Phys. Rev. B* 96, 2017, art. no. 041404(R).

[18] H. T. Dung, L. Knöll, and D.-G. Welsch, Spontaneous decay in the presence of dispersing and absorbing bodies: General theory and application to a spherical cavity, *Phys. Rev. A* 62, 2000, art. no. 053804.

[19] I. Thanopulos, V. Karanikolas, N. Iliopoulos, and E. Paspalakis, Non-Markovian spontaneous emission dynamics of a quantum emitter near a MoS_2 nanodisk, *Phys. Rev. B* 99, 2019, art. no. 195412.

[20] V. D. Karanikolas, C. A. Marocico, and A. L. Bradley, Tunable and long-range energy transfer efficiency through a graphene nanodisk, *Phys. Rev. B* 93, 2016, art. no. 035426.

[21] In case of a disk with radius $R = 7.5$ nm, the fitting procedure results in $\beta = 5.811 \cdot 10^{-4} \pm 7.08 \cdot 10^{-5}$ eV for $\omega_c = 1.956$ eV. We note that these values in both cases are obtained by applying a single peak fitting to $\tilde{J}^{\pm}(\omega)$ using $J^{L}(\omega)$ at the above ω_c values.